


 Cite this: *RSC Adv.*, 2024, 14, 27365

# Rational design of graphdiyne-based single-atom catalysts for electrochemical CO<sub>2</sub> reduction reaction†

 Liyun Jiang, <sup>‡a</sup> Mengdie Zhao <sup>‡b</sup> and Qi Yu\*<sup>‡b</sup>

Graphdiyne (GDY) has achieved great success in the application of two-dimensional carbon materials in recent years due to its excellent electrochemical catalytic capacity. Considering the unique electronic structure of GDY, transition metal (TM<sub>1</sub>) (TM = Fe, Ru, Os, Co, Rh, Ir) single-atom catalysts (SACs) with isolated loading on GDY were designed for electrochemical CO<sub>2</sub> reduction reaction (CO<sub>2</sub>RR) with density functional theoretical (DFT) calculations. The charge density difference and projected densities of states have been systematically calculated. The mechanism of electrochemical catalysis and the reaction pathway of CO<sub>2</sub>RR over Os<sub>1</sub>/GDY catalysts have also been investigated and high catalytic activity was found for the generation of methane. The calculated results provide a theoretical basis for the design of efficient GDY-based SACs for electrochemical CO<sub>2</sub>RR.

 Received 26th June 2024  
 Accepted 18th August 2024

DOI: 10.1039/d4ra04643a

[rsc.li/rsc-advances](http://rsc.li/rsc-advances)

## Introduction

The increasing concentrations of CO<sub>2</sub> in the atmosphere has caused a series of environmental problems such as global warming, extreme weather, and land desertification. Therefore, the efficient conversion and utilization of CO<sub>2</sub> is a current focus of international research.<sup>1–3</sup> Compared to thermal-catalysis, photocatalysis, and biological catalysis, electrocatalysis has certain advantages in terms of economical benefits and the efficiency of electron transfer.<sup>4–9</sup> The industrialization of electrochemical carbon dioxide reduction reactions (CO<sub>2</sub>RR) is a win-win endeavor that can not only reduce carbon dioxide concentrations, but also generate valuable alcohols, ketones, and aldehydes.<sup>10–12</sup> The key is to design catalysts with high efficiency, high selectivity, low cost and easy industrialization.<sup>13–16</sup>

Since Zhang, Li and Liu *et al.* proposed a new concept of single-atom catalyst (SAC) in 2011,<sup>17</sup> the research of which is increasingly extensive in catalysis because of the unique electronic structure and high atomic utilization.<sup>18–24</sup> Although the atom utilization of highly dispersed metal SACs achieves 100%, the large surface energy of metal mono-atoms makes it easy to produce agglomeration effects to form nanoparticles. Therefore, the selection of suitable substrates is key to obtaining

stable metal SACs.<sup>25–28</sup> Compared with conventional metal catalysts, transition metal (TM) atoms have the advantage of controllable coordination geometry of the active center. Due to the geometry, electronic, spin, and magnetic states can be fine-tuned to achieve the desired catalytic activity and selectivity,<sup>29–32</sup> TM SACs have been extensively studied in electrochemistry.<sup>30,33–36</sup> Usually, single atoms of the same period are chosen to be loaded on the catalyst substrate, and based on this, we would like to study the variation between the group VIII B. Six single-atom catalysts Fe, Ru, Os, Co, Rh and Ir were selected for further computational screening of single-atom catalysts that are more suitable for performing CO<sub>2</sub>RR. Among carbon materials, GDY is a new isomer of carbon consisting of both sp<sup>2</sup> and sp-hybrid carbon atoms, in which sp-hybrid carbon atoms can form strong covalent bonds with metal atoms.<sup>37</sup> Metal atoms could exist stably in GDY because of the high electrical conductivity and specific surface area.<sup>38–40</sup> GDY-loaded TM SACs have higher catalytic activity than GDY,<sup>41,42</sup> which has significance for the activity and selectivity of CO<sub>2</sub>RR.

Herein, the stability of SACs loaded with TM<sub>1</sub> (TM<sub>1</sub> = Fe, Ru, Os, Co, Rh, and Ir) on GDY was theoretically investigated by using density functional theoretical (DFT) calculations. Os<sub>1</sub>/GDY was used as a typical to explore the chemical interaction of TM<sub>1</sub> and GDY surface. The electronic structure and electrochemical catalysis properties of Os<sub>1</sub>/GDY for CO<sub>2</sub>RR were investigated in detail.

## Computational details

The classical calculations are based on the spin polarization DFT implemented in the Vienna *ab initio* Simulation Package (VASP).<sup>43,44</sup> Electron exchange and correlation energy are approximated by Perdew–Burke–Ernzerhof (PBE) exchange–

<sup>a</sup>School of Physics and Telecommunication Engineering, Shaanxi University of Technology, Hanzhong 723001, China

<sup>b</sup>School of Materials Science and Engineering, and Shaanxi Laboratory of Catalysis, Shaanxi University of Technology, Hanzhong 723001, China. E-mail: [qiyu@snut.edu.cn](mailto:qiyu@snut.edu.cn)

 † Electronic supplementary information (ESI) available. See DOI: <https://doi.org/10.1039/d4ra04643a>

‡ These authors contributed equally.



correlation functional.<sup>45</sup> Projector augmented wave (PAW) pseudopotential is used to describe the interaction between core and valence electrons,<sup>46</sup> projected electronic densities of states (PDOS),<sup>47</sup> and charge density difference (CDD).<sup>48</sup> GDY cluster is composed of 72 carbon atoms with a cell of  $19.6 \text{ \AA} \times 19.6 \text{ \AA} \times 14 \text{ \AA}$ ,  $\alpha = \beta = 90^\circ$ ,  $\gamma = 60^\circ$ . All carbon atoms in the cell were fully relaxed during the structural optimization, and it stopped the optimization when the force was smaller than  $0.006 \text{ eV \AA}^{-1}$ . The energy cut-off of the plane wave base is set to 620 eV, the electron convergence criterion is  $1 \times 10^{-5} \text{ eV}$ , and the ion relaxation continues until the atomic force is less than  $0.05 \text{ eV \AA}^{-1}$ . The entire calculation is geometrically optimized using a  $3 \times 3 \times 1$  *k*-point density, and the van der Waals (vdW) is evaluated using the DFT-D3 method.<sup>49</sup>

The binding energy ( $E_b$ ) was calculated to check the stability of the TM in GDY. The definition equation is as follows

$$E_b(\text{TM}) = E_{\text{TM}_1/\text{GDY}} - E_{\text{GDY}} - E_{\text{TM}}$$

where  $E_{\text{TM}_1/\text{GDY}}$  is the total energy of the whole system when the single metal atom is in the best adsorption position,  $E_{\text{GDY}}$  is the total energy of GDY substrate,  $E_{\text{TM}}$  is the total energy of the single transition metal atom.

Adsorption energy ( $E_{\text{ad}}$ ) is the energy released by the rate reduction during  $\text{CO}_2$  adsorption. The  $E_{\text{ad}}$  of  $\text{CO}_2$  on  $\text{TM}_1/\text{GDY}-\text{CO}_2$  (TM = Fe, Ru, Os, Co, Rh, Ir) catalyst is calculated to compare the stability of  $\text{CO}_2$  adsorption on different carriers. The adsorption energy is as follows

$$E_{\text{ad}} = E_{\text{TM}_1/\text{GDY}-\text{CO}_2} - E_{\text{TM}_1/\text{GDY}} - E_{\text{CO}_2}$$

Here,  $E_{\text{TM}_1/\text{GDY}-\text{CO}_2}$  is the energy of  $\text{CO}_2$  adsorbed on  $\text{TM}_1/\text{GDY}$  catalyst,  $E_{\text{TM}_1/\text{GDY}}$  is the energy of  $\text{TM}_1/\text{GDY}$  stable structure, and  $E_{\text{CO}_2}$  is the energy of  $\text{CO}_2$  molecule.

The charge transfer before the formation of  $\text{TM}_1/\text{GDY}$  is analyzed by differential charge analysis. The differential charge map is mostly applied to analyze the bonding between atoms of the model after structural optimization in the first nature principle calculations, especially in the interface calculations, where the bonding mode of the interface can be initially visualized by CDD analysis.<sup>50</sup> The common definition of differential charge is

$$\Delta\rho = \rho_{\text{TM}_1/\text{GDY}} - \rho_{\text{GDY}} - \rho_{\text{TM}}$$

where  $\rho_{\text{TM}_1/\text{GDY}}$  denotes the optimized structural charge density of  $\text{TM}_1/\text{GDY}$ ,  $\rho_{\text{GDY}}$  denotes the charge density of the structurally optimized GDY substrate, and  $\rho_{\text{TM}}$  denotes the structural charge density of the transition metal single atom.

The free energy ( $\Delta G$ ) distribution of  $\text{CO}_2\text{RR}$  is described by the computational hydrogen electrode (CHE) model pioneered by Nørskov *et al.*<sup>51,52</sup> In the CHE method,  $\Delta G$  is calculated as follows

$$\Delta G = \Delta E + \Delta E_{\text{ZPE}} - T\Delta S + eU + k_{\text{B}}T \text{pH} \ln 10$$

herein  $\Delta E$  is the total reaction energy,  $\Delta E_{\text{ZPE}}$  is the correction of zero-point energy (ZPE),  $T\Delta S$  is the entropy contribution, and  $eU$

denotes the energy contributed by the applied electrode potential. The pH in our work is set as zero, considering the strong acid environment. The free energy of  $\text{H}^+ + \text{e}^-$  is equal to  $1/2H_2$  under the standard conditions.

## Results and discussion

### Structure and stability of $\text{TM}_1/\text{GDY}$

The protocell of GDY is composed of 18 carbon atoms, six of which are located on a hexagonal ring with  $\text{sp}^2$  hybridization and others on a linear acetylene chain with  $\text{sp}$  hybridization. The network structure of the graphite alkyne has  $\text{C}_6$  hexagon consisting of an acetylene bond linking two adjacent  $\text{sp}^2$ -hybridized carbon atoms.<sup>53,54</sup> The C–C bond length in the hexagon is 1.43 Å, which is alternately distributed as a single bond, a triple bond, and a single bond with bond lengths of 1.40 Å and 1.23 Å.  $\text{TM}_1$  SACs (TM = Fe, Ru, Os, Ni, Rh, and Ir) were loaded and optimized on the optimized GDY. The  $\text{TM}_1/\text{GDY}$  structure with stable adsorption was obtained by screening three possible binding sites for the  $\text{TM}_1$  loading in the GDY including the corner site of the large triangular acetylene ring, the central cavity site of the acetylene ring, and the cavity site above the center of the hexagonal ring. As shown in Fig. 1, it can be seen that all transition metals are located within the cavities of the  $\text{sp}$  bonds in GDY. By measuring the distances between the  $\text{TM}_1$  and the adjacent C atoms, the results are distributed from 1.85 Å to 2.10 Å. Among them, the Rh atom locates with the largest distance of 2.102 Å and the Co atom with the smallest distance of 1.852 Å. Os, Ru, and Ir exhibit a distance of around 1.93 Å ~ 2.07 Å. The distance between Fe and the adjacent carbon atoms is around 1.88 and 1.98 Å, which are shorter than that of Os, Ru, and Ir.

It can be seen from Fig. 2 that the charge density accumulation between the top of Ru and Co atoms and carbon atoms is enhanced, which is weakened for Os. The charge density at the top is also weakened. Charge transfer on GDY occurs mainly from the p-orbital of carbon atoms to the d-orbital of metal atoms. The charge on the vertical orbitals accumulates on Ru and Co, and is consumed on Fe, Os, Rh, and Ir. The results indicate that the charge transfer occurs mainly on the carbon atoms adjacent to the transition metal atoms on GDY, and also on the  $\text{sp}$  hybridized carbon atoms where the  $\text{sp}$  bonds on the benzene rings are involved in the redistribution of the charge density.

The stability of GDY transition metal composites was quantified by measuring the binding energy of GDY-loaded transition metal SACs. The larger the negative value of the binding energy, the more stable the bonding of  $\text{TM}_1$  single-atoms with GDY. As seen from Fig. 3, the binding energy of  $\text{Ru}_1/\text{GDY}$  is  $-3.88 \text{ eV}$ , which is the highest binding energy among the six  $\text{TM}_1$  SACs. But  $\text{Ir}_1/\text{GDY}$  is more stable with a binding energy of  $-4.88 \text{ eV}$ . First-principles adsorption energy calculation is a quantum mechanics-based measurement method that can be applied to materials design, catalyst development, and gas separation. In the development of catalyst, the adsorption capacity and catalytic activity can be scientifically and rationally predicted by calculating the



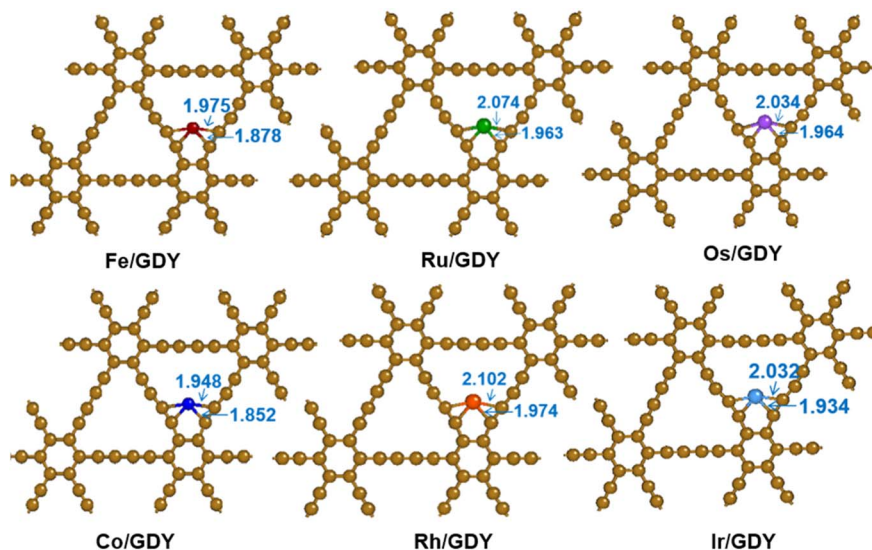


Fig. 1 Optimized  $TM_1/GDY$  geometry ( $TM = Fe, Ru, Os, Ni, Rh, Ir$ ).

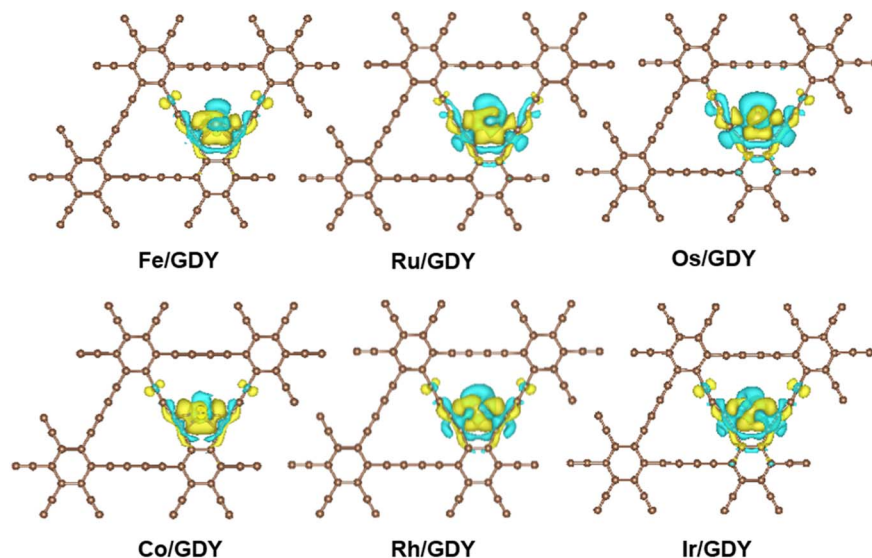


Fig. 2 The CDD of  $TM_1/GDY$ . The yellow and blue equivalence surfaces represent charge accumulation and charge depletion, respectively.

adsorption energies of different catalyst surfaces or interfaces with molecules. It can also help to design and develop new catalysts and continue to optimize their performance. By calculating and comparing the adsorption energies of  $TM_1/GDY$  and  $CO_2$ , the results listed in Fig. 3 showed that  $Os_1/GDY$  has an adsorption energy of  $-1.20$  eV with  $CO_2$  which is the most stable one among the  $TM_1$  SACs.

### Structure of $Os_1/GDY$

The density of states as a visualization result of energy band structure, which can reflect the distribution of electrons in each orbital and reveal the bonding nature between atomic chemical bonds, is a key parameter to further investigate the electronic structure of SACs.<sup>55,56</sup> The spin-polarized PDOS and CDD of  $Os_1/GDY$  and  $Os_1/GDY$  adsorbed  $CO_2$  are calculated and shown in

Fig. 4a, from which we can see that the DOS between the spikes of Os near the Fermi energy level is not zero and the 5d orbital of Os plays a dominant role in bonding with the GDY surface. The pseudopotential gap near the Fermi level due to the p orbitals of C and O in  $CO_2$  interact with the d orbitals of Os indicates that the addition of  $CO_2$  makes the covalence of  $Os_1/GDY$  enhanced and facilitates the further of  $CO_2RR$ . At the same time, the CDD of  $Os_1/GDY$  adsorbed by the stable configuration  $Os_1/GDY$  and  $CO_2$  was investigated (Fig. 4b and c). Because of the doping of transition metal atoms, the system spin polarization becomes larger to promote the activation of  $CO_2$ , and also lead electrons to mainly flow from Os atoms to  $CO_2$  molecules. When  $*CO_2$  is hydrogenated to  $*COOH$ , electrons transfer from H to the lone pair of electrons of  $CO_2$ , which further weakens the C–O bond and makes it more conducive to the subsequent electrocatalysis with  $H^+$ .



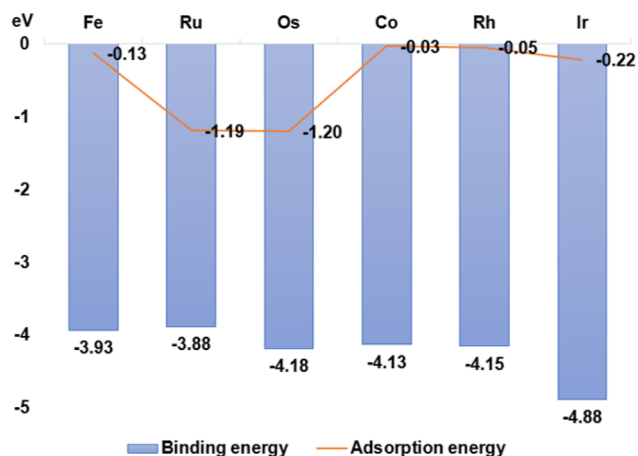


Fig. 3 The binding energy of GDY-loaded Fe, Ru, Os, Co, Rh, and Ir single atoms and CO<sub>2</sub> adsorption energy.

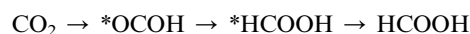
### Hydrogen evolution reaction

The competition between the hydrogen evolution reaction (HER) and CO<sub>2</sub>RR is crucial in aqueous electrolytes because the first step in CO<sub>2</sub>RR is the protonation of CO<sub>2</sub> to \*COOH or \*OCOH, consuming \*H and electrons. And the HER starts with the synthesis of \*H with a catalyst, where \*H and electrons are essential. On TM<sub>1</sub>/GDY, the transition metal interacts with \*H. The predicted overpotential of HER is lower than that of Fe<sub>1</sub>/GDY and Co<sub>1</sub>/GDY. When  $U = 0$  V, Fe<sub>1</sub>/GDY acts as a great HER catalyst candidate (Fig. 5a). As shown in Fig. 5b, we found that the lower free energy changes showed higher selectivity through comparing the adsorption free energy changes ( $\Delta G$ ) of \*CO<sub>2</sub> and \*H. Among them, Fe, Ru, Os, Co, Rh, and Ir are all located below the parity line which defines the selectivity between CO<sub>2</sub>RR and HER. Therefore, the resistance of TM<sub>1</sub>/GDY to HER can be effectively used as CO<sub>2</sub>RR catalysts. The loading of transition metal single-atoms improved the activity and selectivity of CO<sub>2</sub> initial reduction. For Os<sub>1</sub>/GDY, the adsorption of \*CO<sub>2</sub> is better than \*H, which means that it favors to become a catalyst for

CO<sub>2</sub>RR. Because the active site is easily occupied by \*CO<sub>2</sub> and \*CO<sub>2</sub> is more negative than \*H, the Os<sub>1</sub>/GDY catalyst can effectively adsorb and further catalyze CO<sub>2</sub>.

### Electrochemical CO<sub>2</sub>RR

In the CO<sub>2</sub>RR, the C<sub>1</sub> products including CO, HCOOH, CH<sub>4</sub>, and CH<sub>3</sub>OH are frequently generated. CO<sub>2</sub> is first reduced over a catalyst into \*COOH or \*OCOH, which forms \*CO or \*HCOOH by further electrochemical reduction.<sup>57</sup> Followed by desorption of \*CO and \*HCOOH from the SACs, CO and HCOOH is generated, respectively.<sup>58,59</sup>



The basic reaction step of further protonation of \*CO intermediates on the catalyst surface is currently the rate-determining step for most electrocatalysts, and this process may form either \*CHO or \*COH. Peterson *et al.* have concluded that the process of \*CO protonated to form \*CHO would more efficient when the catalyst surface bind both \*CO and \*CHO strongly.<sup>52</sup> The research group of Nie proposed that the final product is strongly dependent on two key intermediates \*CHO and \*COH.<sup>60</sup> If \*CO is protonated to form \*CHO, then \*CHO continues to be protonated to form \*OCH<sub>2</sub> and \*OCH<sub>3</sub>, and the location of further hydrogenation of \*OCH<sub>3</sub> may affect the selectivity of the final product, which eventually forms CH<sub>4</sub> on the catalyst surface.<sup>61</sup> There are usually two pathways to generate CH<sub>4</sub>. Based on studies of the initial reduction of CO<sub>2</sub>, CO<sub>2</sub>RR involves more steps of proton-electron pair transfer, leading to an end product that is often not monolithic.

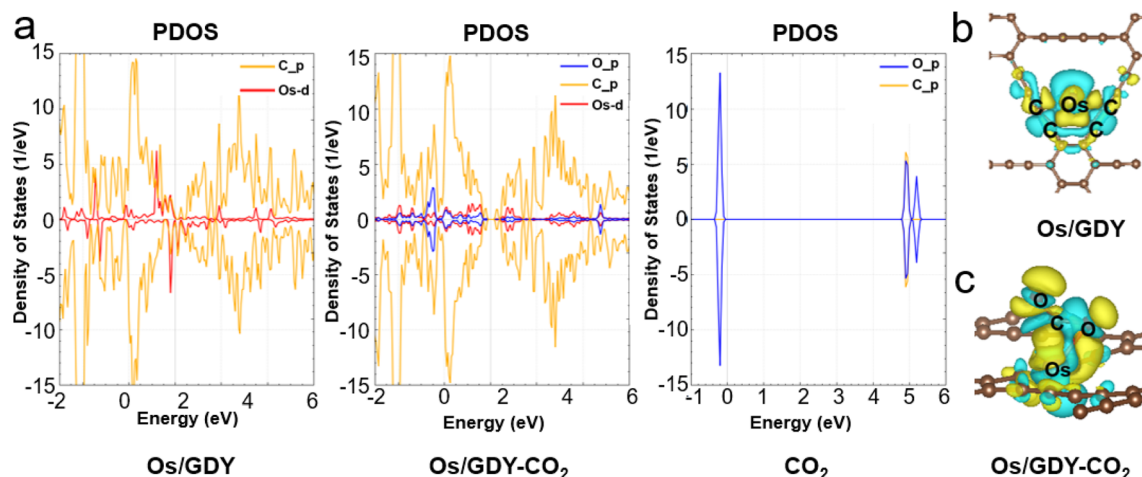
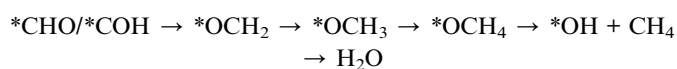


Fig. 4 (a) The schematic diagram of projected electronic densities of states of Os<sub>1</sub>/GDY, Os<sub>1</sub>/GDY-CO<sub>2</sub>, and CO<sub>2</sub>. CDD plots of (b) Os<sub>1</sub>/GDY and (c) Os<sub>1</sub>/GDY-CO<sub>2</sub>.



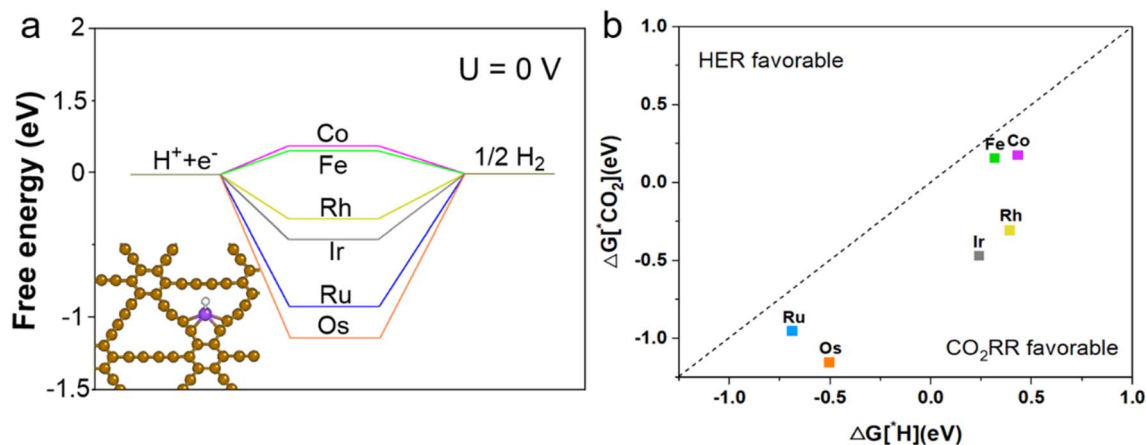


Fig. 5 (a) The free energy diagrams for HER at equilibrium  $U = 0$  V on  $TM_1/GDY$ . (b) The change of  $\Delta G$  in the first protonation step of  $CO_2RR$  adsorption and HER on  $TM_1/GDY$  catalysts. The region below/above the parity test represents  $CO_2RR/HER$  selectivity, respectively.



One process of  $CH_4$  formation is the continuous protonation of C into  $*O$  and  $CH_4$  and the further hydrogenation of  $*O$  to  $H_2O$ . In another process, the O is protonated to form  $H_2O$  and  $*C$ , and then  $*C$  is deoxidized to form  $CH_4$ .<sup>62,63</sup> However, hydrogenation reactions should also be considered for processes that occur between C and O. The free energy pathways involving the protonation of  $*COH$  and  $*CHO$  were shown in Fig. 6. It can be seen that the protonation of  $*CO$  to  $*COH$  on the surface of the  $Os_1/GDY$  catalyst is the step with the maximum free energy variation ( $\Delta G = 0.61$ ), and the protonation of  $*CHO$  to  $*CH_2O$  is the reaction step with the optimal energy. Subsequently,  $*CH_2O$  is more energetically inclined to form  $*CH_3O$  relative to  $*CH_2OH$ . Eventually,  $*CH_3O$  was further protonated to form  $*OCH_4$  intermediates, which further produce  $CH_4$ .

Synthesizing the previous discussion on the electronic structure of  $Os_1/GDY$ , doping Os on GDY changes the charge density and state density, which is more conducive to the adsorption of  $CO_2$ , and thus has better performance for electrocatalytic  $CO_2RR$  to generate  $CH_4$ .

## Conclusions

In this paper, DFT calculations were used to investigate the selectivity of  $CO_2RR$  activity of GDY-loaded transition metal SACs by screening  $TM_1/GDY$  ( $TM = Fe, Ru, Os, Co, Rh,$  and  $Ir$ ) monatomic catalysts. By studying the electronic structure including DOS and CDD, it was found that the sp-hybridized carbon atoms on GDY have a great potential to tune the electronic structure of SACs and participate in the adsorption process of TM. The  $CO_2RR$  of the  $Os_1/GDY$  catalysts showed high performance towards  $CH_4$  with an energy potential barrier of 0.61 eV. Therefore, the GDY-loaded transition metal SAC may be a promising catalyst for application in other reduction reactions.

## Data availability

The data that support the findings of this study are available from the corresponding author upon reasonable request.

## Author contributions

L. J. and M. Z. performed first-principles calculations, data curation, formal analysis and wrote the original draft. Q. Y. obtained funding support, participated in the discussion of the electronic structure calculations used in the paper and reviewed the manuscript.

## Conflicts of interest

The authors declare no competing financial or non-financial interests.

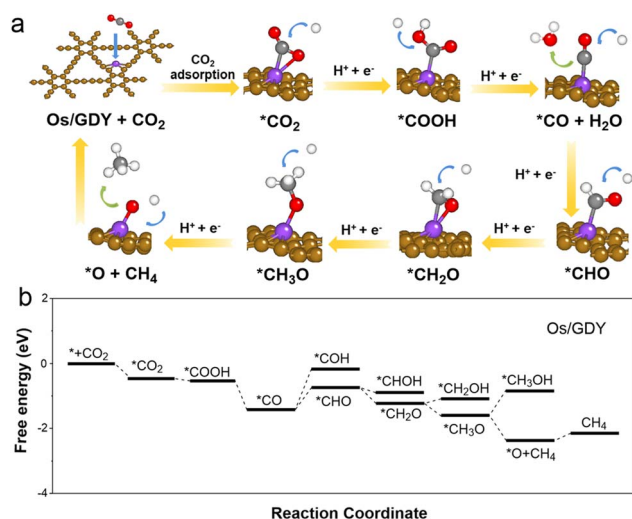


Fig. 6 Reaction mechanism of  $CO_2RR$  to  $CH_4$  on  $Os_1/GDY$ . (a) The structure of the reaction intermediates; (b) different energy profiles. CHE model and the DFT method of PBE functional are used to calculate the path.



## Acknowledgements

This work was financially supported by the National Natural Science Foundation of China (No. 92061109), Natural Science Basic Research Program of Shaanxi (Program No. 2021JCW-20 and 2022KJXX-18). We gratefully acknowledge HZWTECH for providing computation facilities.

## References

- W. Ma, S. Xie, T. Liu, Q. Fan, J. Ye, F. Sun, Z. Jiang, Q. Zhang, J. Cheng and Y. Wang, *Nat. Catal.*, 2020, **3**, 478–487.
- Z. Chen, Z. Liu and X. Xu, *Nat. Commun.*, 2023, **14**, 936.
- T. Theerathanagorn, A. Vidal-Lopez, A. Comas-Vives, A. Poater and V. D'Elia, *Green Chem.*, 2023, 4336–4349.
- M. D. Hossain, Q. Zhang, T. Cheng, W. A. Goddard and Z. Luo, *Carbon*, 2021, **183**, 940–947.
- K. Liu, J. Li, Y. Liu, M. Wang and H. Cui, *J. Energy Chem.*, 2023, 515–534.
- Q. Yu, R. Lin, L. Jiang, J. Wan and C. Chen, *Sci. China Mater.*, 2018, **61**, 1007–1011.
- N. Kornienko, Y. Zhao, C. S. Kley, C. Zhu, D. Kim, S. Lin, C. J. Chang, O. M. Yaghi and P. Yang, *J. Am. Chem. Soc.*, 2015, **137**, 14129–14135.
- Y. Dai and Y. Xiong, *Nano Res. Energy*, 2022, **1**, e9120006.
- J. Yuan, H. Li, Q. Wang, Q. Yu, X. Zhang, H. Yu and Y. Xie, *Mater. Lett.*, 2012, **81**, 123–126.
- S. Zhang, Q. Fan, R. Xia and T. J. Meyer, *Acc. Chem. Res.*, 2020, **53**, 255–264.
- F. P. García de Arquer, C.-T. Dinh, A. Ozden, J. Wicks, C. McCallum, A. R. Kirmani, D.-H. Nam, C. Gabardo, A. Seifitokaldani and X. Wang, *Science*, 2020, **367**, 661–666.
- T. Zheng, K. Jiang and H. Wang, *Adv. Mater.*, 2018, **30**, 1802066.
- Y. Y. Birdja, E. Pérez-Gallent, M. C. Figueiredo, A. J. Göttle, F. Calle-Vallejo and M. T. Koper, *Nat. Energy*, 2019, **4**, 732–745.
- J. Gu, C.-S. Hsu, L. Bai, H. M. Chen and X. Hu, *Science*, 2019, **364**, 1091–1094.
- T. Ahmad, S. Liu, M. Sajid, K. Li, M. Ali, L. Liu and W. Chen, *Nano Res. Energy*, 2022, (1), e9120021.
- Q. Zeng, G. Yang, J. Chen, Q. Zhang, Z. Liu, B. Qin and F. Peng, *Carbon*, 2023, **202**, 1–11.
- B. Qiao, A. Wang, X. Yang, L. F. Allard, Z. Jiang, Y. Cui, J. Liu, J. Li and T. Zhang, *Nat. Chem.*, 2011, **3**, 634–641.
- Q. Yang, Y. Jiang, H. Zhuo, E. M. Mitchell and Q. Yu, *Nano Energy*, 2023, 108404.
- X.-F. Yang, A. Wang, B. Qiao, J. Li, J. Liu and T. Zhang, *Acc. Chem. Res.*, 2013, **46**, 1740–1748.
- Q. Zhang and J. Guan, *Adv. Funct. Mater.*, 2020, **30**, 2000768.
- M. B. Gawande, P. Fornasiero and R. Zbořil, *ACS Catal.*, 2020, **10**, 2231–2259.
- S. Ren, Q. Yu, X. Yu, P. Rong, L. Jiang and J. Jiang, *Sci. China Mater.*, 2020, **63**, 903–920.
- Q. Yu, H. Li, Q. Wang, S. Cheng, L. Jiang, Y. Zhang, T. Ai and C. Guo, *Mater. Lett.*, 2014, **128**, 284–286.
- C. Ye, Y. Zhou, H. Li and Y. Shen, *Green Chem.*, 2023, 3931–3939.
- A. Tripathi and R. Thapa, *Carbon*, 2023, **208**, 330–337.
- Y. Pan, R. Lin, Y. Chen, S. Liu, W. Zhu, X. Cao, W. Chen, K. Wu, W.-C. Cheong and Y. Wang, *J. Am. Chem. Soc.*, 2018, **140**, 4218–4221.
- V. Giulimondi, S. Mitchell and J. Pérez-Ramírez, *ACS Catal.*, 2023, **13**, 2981–2997.
- L. Li, S. Cheng, H. Li, Q. Yu, J. Liu and X. Lv, *Nano-Micro Lett.*, 2010, **2**, 154–159.
- H.-Y. Zhuo, X. Zhang, J.-X. Liang, Q. Yu, H. Xiao and J. Li, *Chem. Rev.*, 2020, **120**, 12315–12341.
- C.-X. Zhao, J.-N. Liu, J. Wang, C. Wang, X. Guo, X.-Y. Li, X. Chen, L. Song, B.-Q. Li and Q. Zhang, *Sci. Adv.*, 2022, **8**, eabn5091.
- Y.-N. Gong, W. Zhong, Y. Li, Y. Qiu, L. Zheng, J. Jiang and H.-L. Jiang, *J. Am. Chem. Soc.*, 2020, **142**, 16723–16731.
- P. Rong, Y.-F. Jiang, Q. Wang, M. Gu, X.-L. Jiang and Q. Yu, *J. Mater. Chem. A*, 2022, **10**, 6231–6241.
- C. Xu, A. Vasileff, Y. Zheng and S. Z. Qiao, *Adv. Mater. Interfaces*, 2021, **8**, 2001904.
- Q. Yu, *Sci. China Mater.*, 2023, **66**, 1079–1088.
- J.-C. Jiang, J.-C. Chen, M.-d. Zhao, Q. Yu, Y.-G. Wang and J. Li, *Nano Res.*, 2022, **15**, 7116–7123.
- Q. An, S. Bo, J. Jiang, C. Gong, H. Su, W. Cheng and Q. Liu, *Advanced Science*, 2023, **10**, 2205031.
- X. Gao, J. Li and Z. Zuo, *Nano Res. Energy*, 2022, **1**, e9120036.
- L. Hui, Y. Xue, H. Yu, Y. Liu, Y. Fang, C. Xing, B. Huang and Y. Li, *J. Am. Chem. Soc.*, 2019, **141**, 10677–10683.
- C. Huang, Y. Li, N. Wang, Y. Xue, Z. Zuo, H. Liu and Y. Li, *Chem. Rev.*, 2018, **118**, 7744–7803.
- P. Jiao, D. Ye, C. Zhu, S. Wu, C. Qin, C. An, N. Hu and Q. Deng, *Nanoscale*, 2022, **14**, 14322–14340.
- X. Li and D. Xing, *J. Phys. Chem. C*, 2019, **123**, 8843–8850.
- T. He, S. K. Matta, G. Will and A. Du, *Small Methods*, 2019, **3**, 1800419.
- G. Kresse and J. Furthmüller, *Phys. Rev. B: Condens. Matter Mater. Phys.*, 1996, **54**, 11169.
- G. Kresse and J. Furthmüller, *Comput. Mater. Sci.*, 1996, **6**, 15–50.
- J. P. Perdew, K. Burke and M. Ernzerhof, *Phys. Rev. Lett.*, 1996, **77**, 3865.
- P. E. Blöchl, *Phys. Rev. B: Condens. Matter Mater. Phys.*, 1994, **50**, 17953.
- H. Försterling and H. Kuhn, *Int. J. Quantum Chem.*, 1968, **2**, 413–430.
- M. D. Kostin, *J. Math. Phys.*, 1991, **32**, 1341–1343.
- S. Grimme, *J. Comput. Chem.*, 2006, **27**, 1787–1799.
- J. Ortiz-Medina, F. López-Urías, H. Terrones, F. Rodríguez-Macías, M. Endo and M. Terrones, *J. Phys. Chem. C*, 2015, **119**, 13972–13978.
- J. K. Nørskov, J. Rossmeisl, A. Logadottir, L. Lindqvist, J. R. Kitchin, T. Bligaard and H. Jonsson, *J. Phys. Chem. B*, 2004, **108**, 17886–17892.
- A. A. Peterson, F. Abild-Pedersen, F. Studt, J. Rossmeisl and J. K. Nørskov, *Energy Environ. Sci.*, 2010, **3**, 1311–1315.



## Paper

- 53 X. Fu, X. Zhao, T. B. Lu, M. Yuan and M. Wang, *Angew. Chem., Int. Ed.*, 2023, **62**, e202219242.
- 54 C. Huang, Y. Zhao and Y. Li, *Adv. Mater.*, 2019, **31**, 1904885.
- 55 J. Gao, D. Nandi and M. Gupta, *J. Appl. Phys.*, 2018, **124**, 014502.
- 56 V. Fung, G. Hu, P. Ganesh and B. G. Sumpter, *Nat. Commun.*, 2021, **12**, 88.
- 57 S. Back and Y. Jung, *ACS Energy Lett.*, 2017, **2**, 969–975.
- 58 J.-H. Jeoung and H. Dobbek, *Science*, 2007, **318**, 1461–1464.
- 59 S. Liu, J. Xiao, X. F. Lu, J. Wang, X. Wang and X. W. Lou, *Angew. Chem., Int. Ed.*, 2019, **58**, 8499–8503.
- 60 X. Nie, M. R. Esopi, M. J. Janik and A. Asthagiri, *Angew. Chem.*, 2013, **125**, 2519–2522.
- 61 X. Nie, W. Luo, M. J. Janik and A. Asthagiri, *J. Catal.*, 2014, **312**, 108–122.
- 62 G. Shi, Y. Xie, L. Du, X. Fu, X. Chen, W. Xie, T. B. Lu, M. Yuan and M. Wang, *Angew. Chem., Int. Ed.*, 2022, **61**, e202203569.
- 63 T. Jitwatanasirikul, T. Roongcharoen, P. Sikam, K. Takahashi, T. Rungrotmongkol and S. Namuangruk, *Adv. Mater. Interfaces*, 2023, 2201904.

